Article ID: 1000-9116(2007)04-0359-11 doi: 10.1007/s11589-007-0359-6

Middle and upper crust shear-wave velocity structure of the Chinese mainland*

FENG Mei[1,2),♣] (冯 梅) AN Mei-jian[1,2)] (安美建)

1) *Institute of Geomechanics*, *Chinese Academy of Geological Sciences*, *Beijing* 100081, *China*
2) *Key Laboratory of Crust Deformation and Processes*, *Chinese Academy of Geological Sciences*, *Beijing* 100081, *China*

Abstract

In order to give a more reliable shallow crust model for the Chinese mainland, the present study collected many short-period surface wave data which are better sensitive to shallow earth structures. Different from traditional two-step surface wave tomography, we developed a new linearized surface wave dispersion inversion method to directly get a 3D S-wave velocity model in the second step instead of inverting for 1D S-velocity profile cell by cell. We convert all the regionalized dispersions into linear constraints for a 3D S-velocity model. Checkerboard tests show that this method can give reasonable results. The distribution of the middle- and upper-crust shear-wave velocity of the Chinese mainland in our model is strongly heterogeneous and related to different geotectonic terrains. Low-velocity anomalies delineated very well most of the major sedimentary basins of China. And the variation of velocities at different depths gives an indication of basement depth of the basins. The western Tethyan tectonic domain (on the west of the 95°E longitude) is characterized by low velocity, while the eastern Tethyan domain does not show obvious low velocity. Since petroleum resources often distribute in sedimentary basins where low-velocity anomaly appears, the low velocity anomalies in the western Tethyan domain may indicate a better petroleum prospect than in its eastern counterpart. Besides, low velocity anomaly in the western Tethyan domain and around the Xing'an orogenic belt may be partly caused by high crustal temperature. The weak low-velocity belt along ~105°E longitude corresponds to the N-S strong seismic belt of central China.

Key words: **surface-wave tomography**; **shear-wave velocity**; **sedimentary basins**; **shallow crust**; **China**
CLC number: P315.3^{+}1 **Document code**: A

Introduction

Our knowledge on earth's deep structure is mainly owed to seismological studies, especially to tomographic studies in recent years. Seismic tomography studies began in the 1970's, but studies obtaining reliable deep structure with good resolution began in the middle of 1980's after a large number of seismic networks had been deployed. With more and more seismic station installations and improvement of research methodology, resulted earth's structure model becomes finer and finer.

As everyone knows, shallow crust (middle- and upper-crust and sedimentary layer) is tightly related to environment (*e.g.*, geo-hazard) and resources (*e.g.*, minerals) sustaining the human beings, so it is very important to carry out seismological study on shallow crust. Most of previous

* **Received** 2006-07-18; **accepted in revised form** 2006-05-15.
Foundation item: National Natural Science Foundation of China (40504011, 40674058); State Special Project of Oil-Gas of the Ministry of Land and Resources (XQ-2004-01).
♣ **Author for correspondence**: mei_feng_cn@yahoo.com.cn

shallow crust studies were on regional or local scale, and research degrees for different regions can be quite different because of local/regional geography environment. For well-studied regions, seismic-wave velocity structures with good resolution have been obtained and show certain correlation with geological structures. But one significant thing we should do is comparing seismic crustal structures of different regions and then extending conclusions extracted in well-studied regions to poor-studied regions. Thus, it is necessary to carry out seismological study of the shallow crust of China on a continental scale.

In the body-wave studies, as influenced by subsequent phases, S-wave phase arrivals normally include large uncertainties, but initial P-wave phases can be easily recognized since they are not influenced by other phases. Therefore, body-wave tomography normally uses P-wave arrival times to derive P-velocity structures. The way to derive S-velocity structure is normally based on surface-wave observations. Generally, a surface-wave tomography is done in two steps: carry out 2-D tomography for all periods, and then invert all regionalized dispersions for 1-D S-wave velocities to finally get 3-D S-velocity structure of the crust and upper mantle. Early, Feng and Teng (1983) carried out surface-wave tomographic study for the whole Eurasian mainland and obtained a 3-D crust and upper mantle structure model for the Chinese mainland. Later, other researchers (SONG *et al*, 1994; Ritzwoller and Levshin, 1998; Villaseñor *et al*, 2001; HE *et al*, 2002; ZHU *et al*, 2002; Huang *et al*, 2003; Yanovskaya and Kozhevnikov, 2003) sequentially carried out surface-wave tomographic studies on the Chinese mainland. These studies help us a lot to understand deep earth's structure of the Chinese mainland. But because they mainly used data from 11 Global Seismographic Network stations in China and other stations in the neighboring countries, their dataset was lack of short-path and short-period signals. Consequently, their models have limited resolution for shallow crust structure. If including enough short-path and short-period signals, surface-wave tomography can give crust structure with more reliable resolution. Therefore, it is necessary to derive shallow crust structures on a continental scale by increasing more seismic stations and collecting more short-period data.

To get fine-resolution middle and upper crust structure for the whole Chinese mainland with surface-wave tomographic method, we collected all teleseismic, regional and local data both recorded by 48 broadband stations of New Chinese Digital Seismological Network (NCDSN), 4 stations in Taiwan, some other stations in the neighboring countries and also by some PASSCAL temporary stations. These data include more short-path and short-period surface wave observations, which consequently improve the reliability of our resulted middle and upper crust structures.

1 Data and processing

The present study on middle- and upper-crust S-velocity structure of China is based on fundamental-mode Rayleigh-wave group velocity observations. The sensitivity of surface waves to deep earth's structures is related to frequencies, *i.e*., high-frequency signals are more sensitive to shallow structures and low-frequency signals are more sensitive to deep structures. As the objective of the present study is shallow structure of the middle and upper crust of the Chinese mainland, we collected many short-period (*i.e*., high-frequency) Rayleigh-wave data. Besides collecting Rayleigh wave data recorded by the 48 stations of NCDSN and 4 stations of Taiwan in 2003~2004, we still collected data from 14 PASSCAL temporary stations deployed in Qinghai-Xizang (Tibetean) Plateau and in NE China. To improve the ray-path coverage in the marginal area of China, we also collected data recorded by 12 stations in China's neighboring countries in

2003~2004. Figure 1a shows great-circle ray-paths, epicenters and seismic stations for Rayleigh waves of 10 s period. From this figure, we can see that for the short period of 10 s, the ray-paths reach up to about 3 000 and the path distribution evenly cover the whole mainland.

Group velocities were processed with a multiple filtering technique (MFT) (Dziewonski *et al*, 1969) using the frequency-time analysis software (Herrmann and Ammon, 2002). During the data processing, we firstly eliminate higher-mode surface waves, body waves and noises with a phase-matched filtering method. Then we used variable filtering factor for different frequencies to ensure similar resolution both in time domain and frequency domain. And finally we chose using instantaneous frequency rather than filter frequency to get much reasonable dispersions. A detail explanation on data processing is referred to Feng *et al* (2004). Information of epicenters and event time required by group velocity calculation are taken from the EHB catalogue (Engdahl *et al*, 1998). Figure 1b shows an example of Rayleigh-wave dispersion processed by MFT. The right side of this figure is the seismic waveforms with higher-mode surface waves, body waves and noises filtered out.

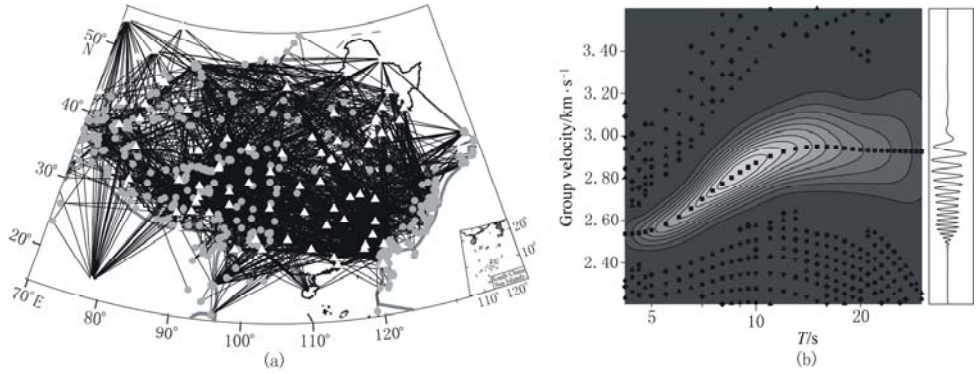

Figure 1 (a) Great-circle ray-paths, epicenters (denoted by circles) and seismic stations (denoted by triangles) for Rayleigh waves of 10 s period; (b) An example of Rayleigh-wave dispersion processed with multiple filtering technique

2 Inversion method

Inversion of group velocities for a 3-D S velocity model is normally broken into two steps: estimation of group velocity maps for different periods and then inversion of regionalized group velocity dispersions for 1-D S velocity models which comprise the final 3-D model (*e.g.*, Shapiro and Ritzwoller, 2002; SU *et al*, 2002; Huang *et al*, 2003; Feng *et al*, 2004). But the second step of this method normally requires strong computation efforts and can hardly introduce lateral smoothness constraints between adjacent cells. To avoid these shortages, we did not use the traditional method but carry out direct 3-D inversion by converting all regionalized dispersions as linearized constraints for the 3-D velocity model.

When inverting for group velocity distribution of different periods, we modelized the studied region (60°~140°E, 15°~55°N) as 1°×1° cells and supposed velocity inside each cell is invariable. So the group-velocity slowness can be obtained by resolving the following objective function (Feng *et al*, 2004):

$$F(\boldsymbol{s}) = \| \boldsymbol{G} \cdot \boldsymbol{s} - \boldsymbol{t}_{\mathrm{o}} \|^2 + \lambda \| \Delta \boldsymbol{s} \|^2 \tag{1}$$

where $\boldsymbol{G}$ is a sensitivity matrix with entries of path-length of each cell; $\boldsymbol{s}$ is the group-velocity slowness vector to be resolved; $\boldsymbol{t}_0$ is the travelling-time vector of observations; $\Delta\boldsymbol{s}$ denotes the first-order gradient of the velocity model that can both smooth the final results and stabilize the large-sparse ill-posed inversion problem; λ is a damping factor of smoothness, *i.e*., bigger λ gives smoother velocity model but with worse travelling-time fitting. So we chose a reasonable damping factor λ by trial and test.

Linearized inversion method is normally used in traditional surface-wave dispersion inversions for 1D shear-wave velocities. An and Assumpção (2006) compared results with linearized inversion method (Snoke and James, 1997), and with neighborhood algorithm (Snoke and Sambridge, 2002) and genetic algorithm (An and Assumpção, 2006) and found that results with nonlinear global methods did not improve too much relative to linearized inversion method. So, after obtaining regionalized dispersions of each cell from the above mentioned method, we converted all the dispersions as linearized constraints of our 3D S-velocity model. We chose IASPEI91 (Kennett and Engdahl, 1991) as the initial model and the model was set with homogeneous layers. As the present study focuses on middle and upper crust structures, layer thickness in crust is set as 5 km, beneath crust layer thickness increases from 10 km to 20 km. For a certain cell, the difference of the regionalized group velocity (U_{R}) and the group velocity of the initial model (U_{iaspei}) can be approximately expressed as a linearized relation to crust thickness (h) and S velocity of each layers (β_i) beneath this cell:

$$\Delta U = U_{\mathrm{R}} - U_{\mathrm{iaspei}} = \frac{\partial U}{\partial h}\Delta h + \sum_{i=1}^{n}\frac{\partial U}{\partial \beta_i}\Delta\beta_i \tag{2}$$

where $\partial U/\partial h$ and $\partial U/\partial\beta_i$ are partial derivatives of group velocities to crust thickness and to S velocity of the i-th layer, respectively. Δh and $\Delta\beta_i$ are perturbations of crust thickness and S velocities relative to the initial model to be resolved. Equation (2) only represents linearized constraint beneath one cell with regionalized dispersion. To realize a direct 3D inversion, we carry out coordinate conversion for the above 1D models to a 3D model and introduce geometrical conversion factors to group velocity partial derivatives (Feng *et al*, 2007). So the final parameters to be resolved become S velocities of all cells at all depths and crust thickness beneath all cells. Such 3D inversion procedure can be easily applied with first-order gradient as smoothness and ensures more reliable results. As shown in equation (2), when calculating partial derivatives to S velocities, we should fix crust thickness and when calculating partial derivatives to crust thickness, we should fix S velocities. So there exists tradeoff between the lower crust velocities and the Moho depth. That is why we do not suggest interpreting lower crust velocities in the present study.

3 Results

To know better about the feasibility of the 3D linear inversion method and the lateral resolution of the inverted results, we carried out a series of checkerboard tests. Figure 2 shows part of the checkerboard test results. Figures 2a and 2b are input S-velocity models with checker size of 4° and 6°, respectively. At all depths, the input anomaly amplitude are set as ±7% relative to the IASPEI91 model. Figures 2c~2h are output S-velocities at different depths (10~20 km). The checkerboard test results show that ray-path distribution directly influences lateral resolution of the inverted results. For example, the central Chinese mainland with dense and homogeneous ray-paths has better lateral resolution than the surrounding mainland and oceans of China which

have relatively poor and inhomogeneous ray-paths. One thing needs to be mentioned is that the lateral resolution at depth of 20 km is similar to depths of 10~15 km, but with weaker anomaly. This might because the depth of 20 km has been partly in middle or lower crust where group

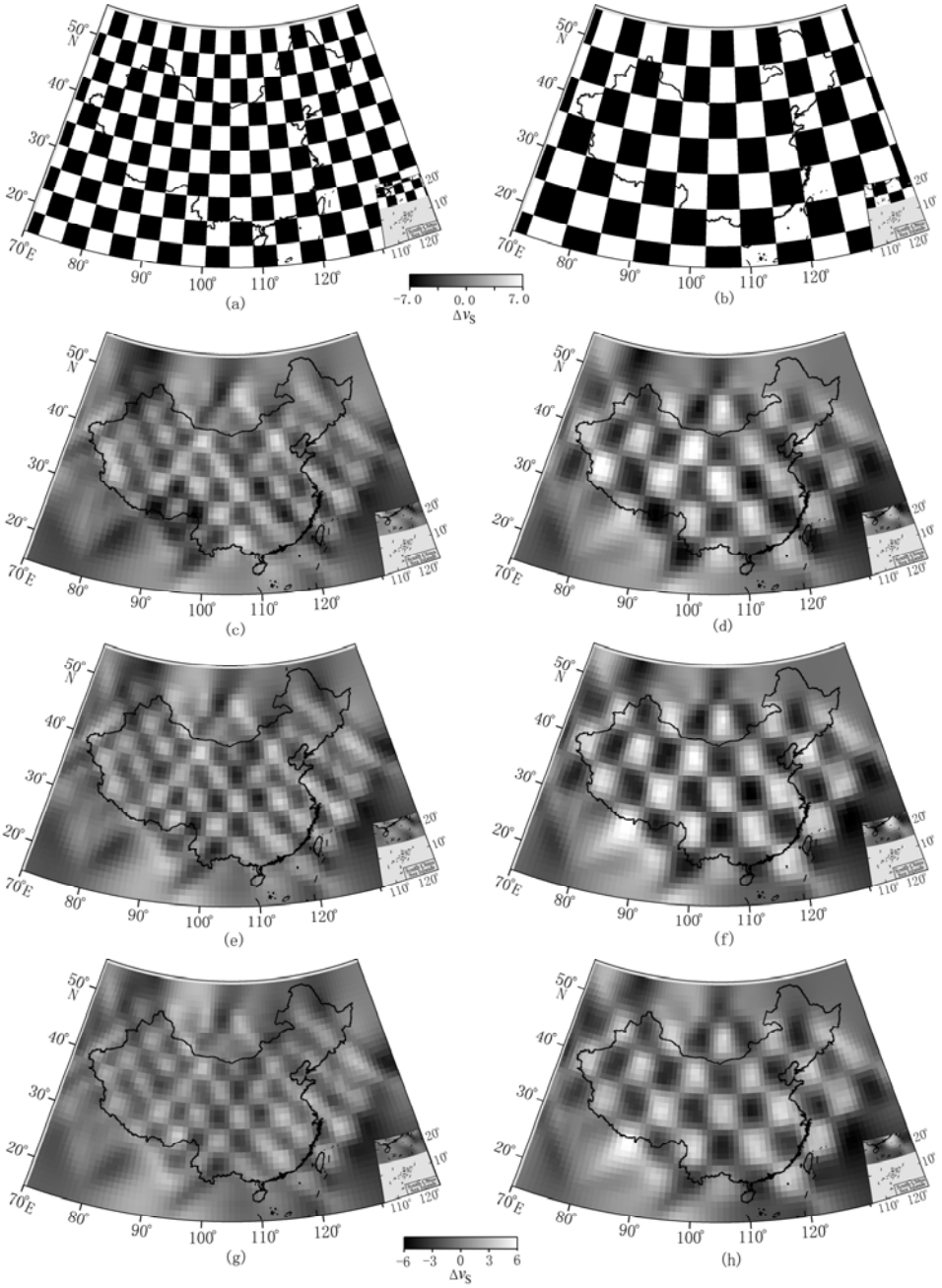

Figure 2 Checkerboard test results

(a) Input S-velocity model with checker size of 4°; (b) Input model with checker size of 6°; (c), (e), (g) are output S-velocity at 10 km, 15 km and 20 km depth for the 4° checkers, respectively; (d), (f), (h) are output S-velocity at 10 km, 15 km and 20 km depth for the 6° checkers, respectively

velocity anomaly can also be interpreted as crust thickness variation. However, because many constraints such as smoothness are normally introduced in seismic tomography, what we concern more is about the velocity anomaly distribution rather than the anomaly amplitude. Comparing lateral resolution of different depths, we can see that the best lateral resolution at all depths is about 3°~4° and the worst is about 5°~6°. These test results also show that our 3D linear inversion method is feasible and reliable.

Figure 3a is Rayleigh wave group velocities for the period of 10 s, where geotectonic boundary data are from REN *et al* (1999). For the central regions with reliable resolution, this figure is generally similar to the group velocity map of 10 s by Huang *et al* (2003). Group velocities of 10 s period mainly reflect average structures above 15 km. From this figure, sediments of the Chinese mainland have an obvious influence on velocity anomalies above 15 km since almost all the sedimentary basins show low group velocities. The distribution and intensity of these low group velocities delineated very well the basins and the relative thickness of sediments. For instance, the Tarim basin with the thickest sediments (Bassin *et al*, 2000) gives the lowest group velocities. Other basins such as Qaidam, Sichuan, Ordos, North China eastern rift basin and Songliao basin all show obvious low group velocities.

Figures 3b~3d are our obtained S-wave velocities at different depths for the Chinese middle-upper crust. As depth of 25 km has been in lower crust in most regions, the three depths shown in Figures 3b~3d generally locate in middle and upper crust. One should note that the map of 10 km depth may include information of sedimentary layers and the map of 20 km depth may be influenced by deep structures. Figure 4 shows vertical transects of velocities crossing through typical regions of the Chinese mainland (locations of transects shown in Figure 3d).

At the depth of 10 km (Figure 3b), the average S-wave velocity of the Chinese mainland is about 3.22 km/s. In this figure, relatively lower velocities (lower than 3.22 km/s) covered almost all the sedimentary basins of China, including Songliao, North China (Bohai basin and Hehuai basin), Sichuan, Qaidam, Tarim and Qiangtang basins, *etc*. Among these basins, the Tarim basin exhibits lowest velocity, and has thickest sediments (Bassin *et al*, 2000; ZHU *et al*, 2006). So, there may be a relation that lower velocity anomaly corresponds to thicker sediments. According to this suggested relation and comparing amplitude of low velocities at 10 km depth, one can tell that sediments of the Qaidam basin and the Songliao basin could be the thinnest, and sediment thickness of the Ordos, North China and Sichuan basins could be thicker than the Songliao basin and thinner than the Tarim basin. Another feature is that the Xing'an orogenic belt has similar low-velocity anomaly to the Songliao basin, which will be discussed later.

The average S-velocity at 15 km (Figure 3c) reaches about 3.32 km/s. Compared with the depth of 10 km, some velocity anomaly changed. Low velocities of two stable regions (Ordos basin and Sichuan basin) become weaker from 10 km to 15 km depth. The Sino-Korean craton can be divided into three blocks: Ordos basin, North China uplift belt and North China eastern rift basin (JIA and ZHANG, 2005). In our results, from depth 10 km to 15 km, the boundary of these three blocks becomes clearer. And the central North China uplift belt shows quite different velocities from the two basins in its east and west.

The average velocity of 20 km depth (Figure 3d) increases to about 3.38 km/s. Generally, though the North China basin, Tarim basin and Qiangtang basin still show low velocities; compared with the depth of 15 km, low velocity of most basins strongly weakens. This indicates that the influence of the sediments on velocities becomes very weak and basement compositions play an important role on the velocities in these areas. Another remarkable feature is that there is a north

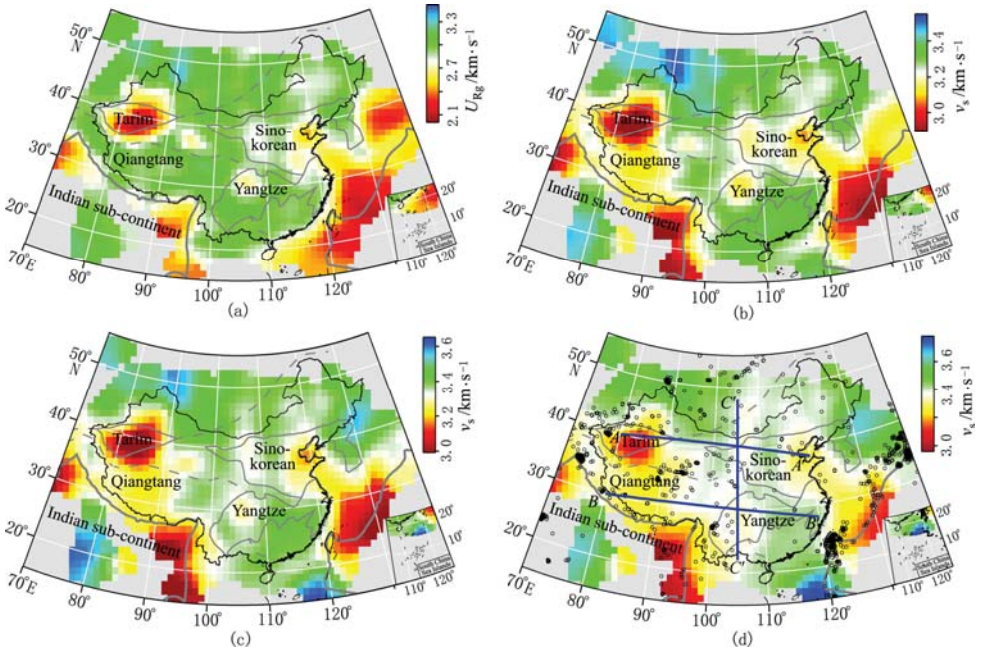

Figure 3 (a) Rayleigh wave group velocities for period of 10 s; (b), (c), (d) are our resulted shear-wave velocities at depth of 10 km, 15 km, and 20 km, respectively

In Figure 3d, small circles indicate epicenters of earthquakes shallower than 20 km occurred since 1990; three blue lines are locations for three vertical velocity transects to be shown in Figure 4

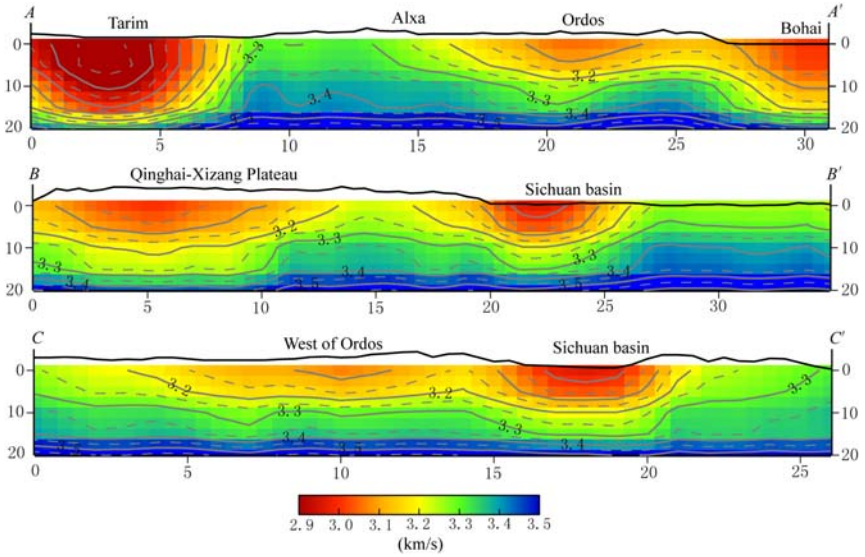

Figure 4 Three vertical transects crossing through the final 3D S-velocity model

Locations of the three transects are shown in Figure 3d. Solid lines close to the surface are exaggerated topography

to south weak low-velocity belt roughly along the 105ºE longitude in the central China. Compared with the north to south strong seismic belt in central China (ZHANG *et al*, 2003), the weak

low-velocity belt exactly overlaps the strong seismic belt on the west of South China block and between the west of Ordos and Alxa block.

Though the checkerboard test shows worse resolution in the eastern oceanic area than in the continental area, all depths show stable velocity structures. Separated by Taiwan, the East China Sea and Yellow Sea in the north show relatively low velocity anomalies, while the South China Sea does not.

From view of vertical transects, transect *AA*' (Figure 4a) crosses from west to east through the Tarim basin, Alxa block, Ordos basin and Bohai basin in the north of China. Velocities lower than 3.1 km/s mainly distribute beneath sedimentary basins, and the depth where such low velocities extend approximately indicates the basement top of the sedimentary basins. Figure 4a indicates that the Tarim basin has thickest sediments; the next is the Bohai basin; the thinnest is the Ordos basin. These results are well consistent with the compilation of ZHU *et al* (2006). Besides the above basins, Figure 4a also implies that the Alxa terrain has not obvious sediments, and the North China uplift zone between the Ordos and Bohai has very thin sediments. Transect *BB*' (Figure 4b) crosses from west to east through the Qinghai-Xizang (Tibet) Plateau, Sichuan basin and southeastern China. The velocities in the transect imply that the western Qinghai-Xizang (Tibet) Plateau and Sichuan basin have obvious sediments while the eastern Tethyan tectonic domain between them does not. The eastern circum-Pacific tectonic domain to the east of Sichuan basin also has no obvious sediments. Transect *CC*' (Figure 4c) crosses from north to south through central China. In Figure 4c, regions to the west of Ordos have thinner sediments than the Sichuan basin. Most velocities at 20 km depth in all the three transects reach 3.5 km/s.

4 Discussion

Seismic velocities of shallow crust are determined by many factors. First, different geotectonics have quite different sediment thickness and rock compositions at shallow depths. Second, structural fractures and porous fluid have strong influences on seismic velocities in shallow depth. Third, from earth's surface to deep, porosity decreases but temperature increases, so temperature becomes one of the important factors influencing seismic velocities in the deep. Therefore, the seismic velocities we obtained here down to 20 km are not only related to different geotectonic units, but also to structural fractures and middle- to upper-crust thermal activities.

In our results, most regions with low-velocity anomaly correlate well with the main sedimentary basins of China, so sediments of these basins is the main reason for low shear-wave velocities. Besides, another feature should be noted is that western Qinghai-Xizang Plateau is not a large sedimentary basin but is characterized by low velocities in depths of 10~20 km. The Igneous Rock Map of China from the Chinese Geological Survey (2006) shows that the western Tibet has widely-distributed Cenozoic volcanic outcrops. In other word, this area occurred magma thermal events during Cenozoic. Heat flow observations (WANG and HUANG, 1990; Pollack *et al*, 1993; HU *et al*, 2001) in these areas though are very limited but all show high heat flow. Therefore, relatively high crustal temperature could be one of the factors resulting in such low crustal velocities in the western Tibet. On the other hand, since the Qinghai-Xizang region is seldom investigated geologically and the sediment thickness is poorly constrained by current data. Considering the correspondence between low velocity and sediments, the low velocities in the Qiangtang basin may indicate existence of widely distributed thick sediments.

Since most of the petroleum productive regions of China are located in sedimentary basins which are characterized by low velocity anomaly at depths of 10~15 km in our results, we can

suppose that regions with low velocity anomalies may have good petroleum prospect. For the whole Tethyan tectonic domain, as the western part separated by the 95°E longitude has low velocities while the eastern part has normal to high velocities, so the western part may have better petroleum prospect than the eastern part. Such conclusion is consistent with recent petroleum exploration results in the Qinghai-Xizang Plateau, *e.g*., the western Qiangtang basin has found some traces of petroleum resources (JIANG, 2005; MA *et al*, 2005), while the eastern region of Songpan-Aba did not yet (MA *et al*, 2005).

The other region with Cenozoic igneous outcrops is the Xing'an orogenic belt to the west of Songliao basin. If simply considering the relations between sediments and velocity anomaly, the Songliao basin should have lower velocity anomaly than the Xing'an orogenic belt where there is less sediment. But our results showed similar low velocity for the two areas. Since there exist Cenozoic igneous outcrops in the Xing'an orogenic belt, the lower velocities may be caused by high crustal temperatures due to regional magma activities.

The upper crust of East China Sea in the north is characterized with low velocity while South China Sea in the south with high velocity. This feature may be partly related to sediments, but more reasonable explanation could be different crustal temperatures caused by different subducting mode between adjacent plates. To the north of Taiwan, the Pacific Plate is subducting westward beneath the Eurasian mainland. The East China Sea and the Yellow Sea are back-arc marginal-sea basins above the subduction slab, so they may have higher crustal temperature. While to the south of Taiwan, the Eurasian Plate is subducting eastward beneath the Philippine Plate (Tsai *et al*, 1977), so the Philippine Plate should have higher crustal temperature, but the Eurasian Plate did not.

Small circles in Figure 3d indicate epicenters of earthquakes since 1990 with depths smaller than 20 km. This figure shows that shallow earthquakes mainly distribute around regions with strong velocity variations, such as the surrounding regions of the low velocity sedimentary basins (Tarim, Ordos, North China eastern rift basins, *etc*) and high velocity regions (eastern Tethyan tectonic domain).

5 Conclusions

Instead of inverting regionalized dispersions cell by cell in the second step of traditional surface-wave tomography, the present study used a 3D inversion method. We converted all the regionalized dispersions to linear constraints for a 3D model and then carried out 3D inversion directly. Checkerboard tests showed that this method can give reasonable results in 10~20 km deep.

Our low velocity anomaly delineated very well the sedimentary basins of the Chinese mainland. The amplitude and extension of the low velocity anomalies reflect somewhat the sediment thickness. For instance, the Tarim basin with very thick sediment shows strong low velocity in our results. Generally, low velocity anomalies may have different origins. For sedimentary basins, low velocities are probably caused by thick sediments, while for other regions like Qiangtang basin and its surrounding Qinghai-Xizang regions, the low velocities may be partly caused by sediments and partly caused by high crustal temperatures. For the Xing'an orogenic belt where there are no obvious sediments and the oceanic area of the East China Sea, the low upper-crust velocities may be principally caused by high temperatures. The western Tethyan tectonic domain separated by the 95°E longitude shows obvious low velocity anomaly; while the eastern part does not show any low velocities. This may indicate that the western Tethyan domain has thicker sedi-

ments and better petroleum prospect than the eastern part.

Acknowledgements We thank Prof. HUANG Zhong-xian and other anonymous reviewers for valuable comments. We also thank China Earthquake Data Center and DMC of IRIS for offering the seismic data. All figures (except Figure 1b) are made with Generic Mapping Tool.

References

An M and Assumpção M S. 2006. Crustal and upper mantle structure in intracratonic Paraná basin, SE Brazil, from surface wave dispersion using genetic algorithm [J]. *J South Amer Earth Sci*, **21**(3): 173-184.

Bassin C, Laske G, Masters G. 2000. The current limits of resolution for surface wave tomography in North America [J]. *EOS Trans AGU*, **81**: F897.

Chinese Geological Survey. [2006]. Igneous rock map of China [EB/OL]. [2006-12-20]. http://www.cgs.gov.cn/info/kp/web/KB/earthday1/huoshanyan.htm.

Dziewonski A, Bloch S, Landisman M. 1969. A technique for analysis of transient seismic signals [J]. *Bull Seism Soc Amer*, **59**(1): 427-444.

Engdahl E R, van der Hilst R D, Buland R. 1998. Global teleseismic earthquake relocation with improved travel times and procedures for depth determination [J]. *Bull Seism Soc Amer*, **88**: 722-743.

Feng C C and Teng T L. 1983. Three-dimensional crust and upper mantle structure of the Eurasian continent [J]. *J Geophys Res*, **88**: 2 261-2 271.

Feng M, Assumpção M S, van der Lee S. 2004. Group-velocity tomography and lithospheric S-velocity structure of the South American continent [J]. *Phys Earth Planet Inter*, **147**: 315-331.

Feng M, Van der Lee S, Assumpção M. 2007. Upper mantle structure of South America from joint inversion of waveforms and fundamental-mode group velocities of Rayleigh waves [J]. *J Geophys Res*, **112**: B04312, doi: 10.1029/2006JB004449.

HE Zheng-qin, DING Zhi-feng, YE Tai-lan, *et al.* 2002. Group velocity distribution of Rayleigh waves and crustal and upper mantle velocity structure of the Chinese mainland and its vicinity [J]. *Acta Seismologica Sinica*, **15**(3): 269-275.

Herrmann R B and Ammon C J. 2002. Computer programs in seismology-surface waves, receiver functions and crustal structure [EB/OL]. [2006-12-20]. http://www.eas.slu.edu/People/RBHerrmann/ComputerPrograms.html.

HU Sheng-biao, HE Li-juan, WANG Ji-yang. 2001. Compilation of heat flow data in the China continental area (3rd edition) [J]. *Chinese J Geophys*, **44**(5): 604-618.

Huang Z, Su W, Peng Y, *et al.* 2003. Rayleigh wave tomography of China and adjacent regions [J]. *J Geophys Res*, **108**(B2): 2 073, doi: 10.1029/2001JB001696.

JIA Shi-xu and ZHANG Xian-kang. 2005. Crustal structure and comparison of different tectonic blocks in North China [J]. *Chinese J Geophys*, **48**(3): 672-683.

JIANG Zhong-ti. 2005. Petroleum resources prospect and exploration direction of the Qinghai-Tibet plateau[C]//QIAO De-wu, REN Shou-mai, JIN Chun-shuang, *et al. Symposium of Theory and Technology of Strategic Prospect of Oil and Gas Resources*. Xiamen: Strategic Research Center of Oil and Gas Resources, Ministry of Land and Resources: 70 (in Chinese).

Kennett B L N and Engdahl E R. 1991. Traveltimes for global earthquake location and phase identification [J]. *Geophys J Int*, **105**: 429-465.

MA Yong-sheng, CHEN Yue-kun, SU Shu-an, *et al.* 2005. Progress and preliminary evaluation of oil and gas exploration in Songpan-Aba area[C]//QIAO De-wu, REN Shou-mai, JIN Chun-shuang, *et al. Symposium of Theory and Technology of Strategic Prospect of Oil and Gas Resources*. Xiamen: Strategic Research Center of Oil and Gas Resources, Ministry of Land and Resources: 35-40 (in Chinese).

Pollack H, Hurter S, Johnson J. 1993. Heat flow from the Earth's interior: Analysis of the global data set [J]. *Rev Geophys*, **31**(3): 267-280.

REN Ji-shun, WANG Zuo-xun, CHEN Bing-wei, *et al.* 1999. *The Tectonics of China from a Global View — A Guide to the Tectonic Map of China and Adjacent Regions* [M]. Beijing: Geological Publishing House: 1-50 (in Chinese).

Ritzwoller M H and Levshin A L. 1998. Eurasian surface wave tomography: Group velocities [J]. *J Geophys Res*, **103**(B3): 4 839-4 878.

Shapiro N M and Ritzwoller M H. 2002. Monte-Carlo inversion for a global shear-velocity model of the crust and upper mantle [J]. *Geophys J Int*, **151**: 88-105.

Snoke J A and James D E. 1997. Lithospheric structure of the Chaco and Paraná Basins of South America from surface-wave inversion [J]. *J Geophys Res*, **102**: 2 939-2 951.

Snoke J A and Sambridge M. 2002. Constraints on the S wave velocity structure in a continental shield from surface wave data: Comparing linearized least squares inversion and the direct search neighbourhood algorithm [J]. *J Geophys Res*, **107**(B5): 2094, doi: 10.1029/2001JB000498.

SONG Zhong-he, AN Chang-qiang, CHEN Guo-ying, *et al.* 1994. 3D S-wave velocity structure of the crust and upper mantle [J]. *Science in China* (*Ser B*), **37**(1): 106-118.

SU Wei, PENG Yan-ju, ZHENG Yue-jun, *et al.* 2002. Crust and upper mantle shear velocity structure beneath the Tibetan Plateau and adjacent areas [J]. *Acta Geoscientia Sinica*, **23**(3): 193-200 (in Chinese).

Tsai Y B, Ten T L, Chiu J M, *et al.* 1977. Tectonics implications of the seismicity in the Taiwan region [J]. *Mem Geol Soc China*, **2**: 13-41.

Villaseñor A, Ritzwoller M H, Levshin A L, *et al.* 2001. Shear velocity structure of central Eurasia from inversion of surface wave velocities [J]. *Phys Earth Planet Inter*, **123**: 169-184.

WANG Ji-yang and HUANG Shao-peng. 1990. Compilation of heat flow data in the China continental area (2nd edition) [J]. *Seismology and Geology*, **12**(4): 351-366 (in Chinese).

Yanovskaya T B and Kozhevnikov V M. 2003. 3D S-wave velocity pattern in the upper mantle beneath the continent of Asia from Rayleigh wave data [J]. *Phys Earth Planet Inter*, **138**: 263-278.

ZHANG Pei-zhen, DENG Qi-dong, ZHANG Guo-min, *et al.* 2003. Active tectonic blocks and strong earthquakes in the mainland of China [J]. *Science in China* (*Ser D*), **46**(Suppl. 2): 13-24.

ZHU Jie-shou, CAI Xue-lin, CAO Jia-min, *et al.* 2006. Lithospheric structure and geodynamics in China and its adjacent areas [J]. *Geology in China*, **33**(4): 793-802 (in Chinese).

ZHU Jie-shou, CAO Jia-min, CAI Xue-lin, *et al.* 2002. High resolution surface wave tomography in East Asia and West Pacific marginal seas [J]. *Chinese J Geophys*, **45**(5): 679-698.